Evaporation-residue-gated spin distribution measurements of the highly fissile compound nucleus ^{224}Th* through ^{16}O + ^{208}Pb and ^{18}O + ^{206}Pb reactions

M. M. Hosamani,[1,*] N. M. Badiger,[1] N. Madhavan,[2] I. Mazumdar,[3] S. Nath,[2] J. Gehlot,[2] A. K. Sinha,[4] S. M. Patel,[3] P. B. Chavan,[3] T. Varughese,[2] Vishal Srivastava,[2,†] Md. Moin Shaikh,[2,‡] P. Sandya Devi,[5] P. V. Laveen,[6] A. Shamlath,[6] M. Shareef,[6] S. K. Duggi,[5] P. V. Madhusudhana Rao,[5] G. Naga Jyothi,[5] A. Tejaswi,[5] P. N. Patil,[1] A. Vinayak,[1] K. K. Rajesh,[7] Abhishek Yadav,[2,§] A. Parihari,[2] Rohan Biswas,[2] Monalisha Dhibar,[8] D. P. Kaur,[9] M. Ratna Raju,[5] and J. Joseph[10]

[1]*Department of Studies in Physics, Karnatak University, Dharwad - 580003, India*
[2]*Inter-University Accelerator Centre, Aruna Asaf Ali Marg, New Delhi - 110067, India*
[3]*Tata Institute of Fundamental Research, Mumbai - 400005, India*
[4]*UGC-DAE Consortium for Scientific Research, Kolkata Centre, Kolkata 700098, India*
[5]*Department of Nuclear Physics, Andhra University, Visakhapatnam - 530003, India*
[6]*Department of Physics, Central University of Kerala, Kasaragod - 671314, India*
[7]*Department of Physics, University of Calicut, Kerala - 673635, India*
[8]*Department of Physics, Indian Institute of Technology, Roorkee - 247667, India*
[9]*Department of Physics, Panjab University, Chandigarh - 160014, India*
[10]*Kuriakose Elias College, Mannanam, Kerala - 686561, India*

(Received 5 June 2019; revised manuscript received 19 November 2019; published 23 January 2020)

Measurements of cross sections of evaporation residue (ER) and spin distributions of heavy nuclei, produced via compound nuclear fusion-evaporation reactions, provide crucial information about the dynamics of nuclear fission and the survival probability of the system against fission. Such measurements help in probing the evolution of the compound system from equilibrium to the saddle and the underlying role of nuclear dissipation in hindering fission. The purpose of the present measurements is to understand the survival probability of the ^{224}Th* compound nucleus against fission and its dependence on angular momentum. Measurements of the ER cross sections and spin distributions have been carried out for the ^{16}O + ^{208}Pb and ^{18}O + ^{206}Pb reactions which form the same ^{224}Th* compound nucleus. The two reactions have been carried out at laboratory energies ranging from 87 MeV to 122.6 MeV and 85.7 MeV to 121.4 MeV, respectively. The measurements have been performed at Inter University Accelerator Centre, New Delhi using the Hybrid Recoil mass Analyzer in gas-filled mode, coupled with the 4π spin spectrometer of Tata Institute of Fundamental Research. The reduced ER cross sections ($\sigma_{ER}/\pi R_B{}^2$) for both systems are comparable at low excitation energies while at higher excitation energies the ^{18}O + ^{206}Pb system shows nearly 50% higher values. However, the ^{18}O + ^{206}Pb system shows lower mean γ ray multiplicity (and hence lower mean angular momentum) at all excitation energies which is a surprising result.

DOI: 10.1103/PhysRevC.101.014616

I. INTRODUCTION

Heavy-ion-induced nuclear fusion-evaporation reaction is a well established tool to understand the nuclear dynamics at different stages of fusion-fission process and the associated time-scale. The dynamic properties of a fused compound nuclear system can be studied by measuring the evaporation spectra of neutrons, charged particles, giant dipole resonance (GDR) γ rays and evaporation residues (ERs). The evolution of the compound system from the initial equilibrium state to the scission point as a function of the deformation can be mapped by studying the different evaporation spectra. The emitted particle/radiation (charged particles, neutrons, and γ rays) also serve as clocks for the dynamically evolving system. The observed excess of pre-scission particles and GDR γ rays in comparison with standard statistical model predictions indicates hindrance to the fission process. Frobrich *et al.* [1] pointed out that ERs are the most sensitive and suitable probes for studying the dynamics of fusion-fission process in pre-saddle region. The hindrance in nuclear fission process due to nuclear viscosity increases the pre-saddle and/or pre-scission life time of compound nucleus (CN) and leads to enhanced yields of evaporation residues. Therefore, measurements of ER cross sections and spin distributions would, undoubtedly, provide the necessary information on nuclear fission and the possible role of nuclear viscosity hindering it. It is also understood that the ER production cross section is the only

*mutturajh735@gmail.com
†Present address: Racah Institute of Physics, The Hebrew University of Jerusalem, Jerusalem - 91904, Israel.
‡Present address: Variable Energy Cyclotron Centre, 1/AF, Bidhan Nagar, Kolkata - 700064, India.
§Present address: Department of Physics, Jamia Millia Islamia, New Delhi - 110025, India.

parameter to understand the synthesis of super heavy element (SHE). In this work we report about measurements of ER cross sections and spin distributions for the ^{224}Th compound system for two different projectile-target combinations. Fusion-evaporation reaction of $^{16}O + ^{208}Pb$ system has been studied by several groups over the last two decades, ostensibly, to study fusion-fission and fission hindrance processes. The measurements have covered, high energy giant dipole resonance (GDR) γ rays [2,3], neutrons [4], charged particles [5,6], evaporation residues [7–11], and fission fragments [10,11]. It is now well established from all these measurements that there is an enhanced yield of the pre-scission particle emission compared to what is predicted by standard statistical model based upon phase space considerations. It is, therefore, in place to justify revisiting this system for measuring the ER cross sections and spin distributions. An enhanced yield of ERs indicates enhanced survival probability of the CN against fission and in turn, a reduction in fission width or increased fission life time. This delay in fission can be attributed to nuclear viscosity [12]. As mentioned before, several authors have reported measurements of ER cross sections for the ^{224}Th CN system using the $^{16}O + ^{208}Pb$ reaction. Morton *et al.* [11] used the catcher foil technique to estimate ER cross sections from the α decay of the ERs. Brinkmann *et al.* [10] used deflector plates to select and detect the ERs. Prior to that, Vulgaris *et al.* [9] used a recoil mass separator (RMS) of electric deflector plates, a Wien ($\mathbf{E}\times\mathbf{B}$) filter and two sets of magnetic quadrupole doublets to measure the ER cross sections. It is worth noting that all these techniques are different in nature and there is considerable discrepancy in the ER cross sections extracted by these groups. This causes serious problem for comparison with theoretical calculations. In addition, it is also important to note that no experimental data on ER gated spin distributions have been reported so far for this compound system. The dynamics of the formation and decay of the CN crucially depends upon angular momentum and it is required to measure the ER gated spin distributions and also ER cross sections. Driven by this motive, we have carried out measurements of the evaporation residue cross sections and evaporation residue gated spin distributions for the $^{16}O + ^{208}Pb$ reaction. In addition, we have also performed the same measurements for the $^{18}O + ^{206}Pb$ reaction. There is no data for ER cross sections or spin distributions, for the $^{18}O + ^{206}Pb$ reaction. As mentioned earlier, our primary objective has been to understand the survival probability of the CN against fission and fission hindrance in $^{224}Th^*$ by measuring ER cross sections and spin distributions. The purpose of the second reaction, namely, $^{18}O + ^{206}Pb$ reaction, is to probe any possible difference in the ER spectra due to nominal change of the projectile and target combination, transfer Q values, etc. From purely structure point of view, in the ^{16}O induced reaction both the projectile and target are doubly magic while in the ^{18}O induced reaction neither is doubly magic. The barrier radii for these two reactions, as calculated by the Bass model, are 10.55 and 10.80 fm for the $^{16}O + ^{208}Pb$ and $^{18}O + ^{206}Pb$ reactions, respectively. As both reactions lead to the same compound nucleus it would be interesting to look for any difference in the decay patterns (residue cross sections) of the compound nuclei produced in the two reactions. It is worth noting that recent calculations by Nasirov *et al.*, have tried to explain the difference in evaporation residue cross sections from two reactions, $^{34}S + ^{208}Pb$ and $^{36}S + ^{206}Pb$ leading to the same compound nucleus [13].

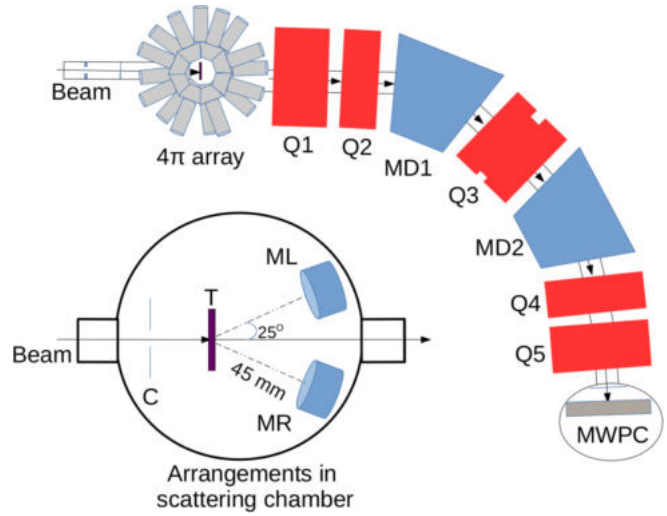

FIG. 1. A schematic representation of the experimental setup; 4π spin spectrometer array (4π array) coupled with the HYRA recoil mass separator. Q1, Q2, Q3, Q4, Q5 are the magnetic quadruples; MD1, MD2 are the magnetic dipoles; MWPC is the focal plane detector; C and T are the collimator and target placed in the beam direction at scattering chamber; ML and MR are the monitor detectors at right and left side of the beam direction.

The organization of the article is as follows. Section II describes the experimental details. The data analysis and extraction of transmission efficiencies of the spectrometers to evaluate the ER cross sections and spin distributions are explained in Sec. III. The last section (Sec. IV) contains the summary and conclusions.

II. EXPERIMENTAL DETAILS

The measurements were carried out at IUAC, New Delhi for the two reactions using the HYbrid Recoil mass Analyzer (HYRA) in gas-filled mode [14] coupled with the TIFR 4π spin spectrometer [15,16]. The schematic representation of the experimental setup is shown in Fig. 1. The pulsed beams of ^{16}O and ^{18}O were provided by the 15UD Pelletron accelerator and the first of three modules of the LINAC accelerator at IUAC. The measurements of the $^{16}O + ^{208}Pb$ system were carried out for the laboratory energies 87, 93.2, 99.3, 105.5, 113.5, and 122.6 MeV with 4 μs pulse separation. For the $^{18}O + ^{206}Pb$ system, after ensuring no contamination of beam-like and target-like particles in the ER spectrum, we reduced the pulse separation from 4 μs to 2 μs in order to improve the intensity of the ^{18}O beam. The average beam intensity (current) throughout the experiment for all energies was $\approx$1 to 2 pnA. Figure 2 shows a typical two-dimensional spectrum of energy versus time of arrival of the ERs. The ER cross sections and spin distribution measurements of de-exciting $^{224}Th^*$ formed by $^{18}O + ^{206}Pb$ were also carried out at the same excitation energies as the previous system

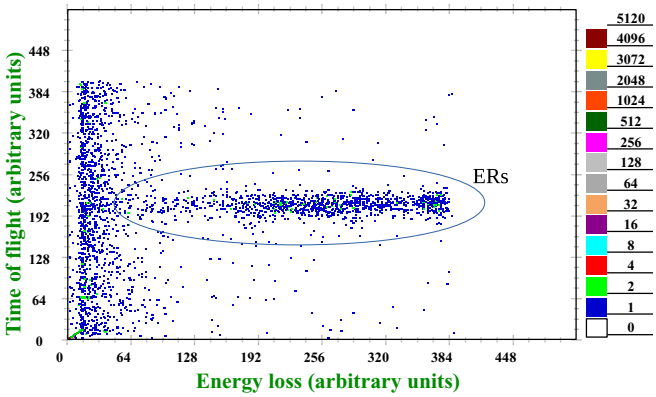

FIG. 2. A typical two-dimensional spectrum of ERs for the system $^{16}O + {}^{208}Pb$ at $E_{lab} = 122.6$ MeV.

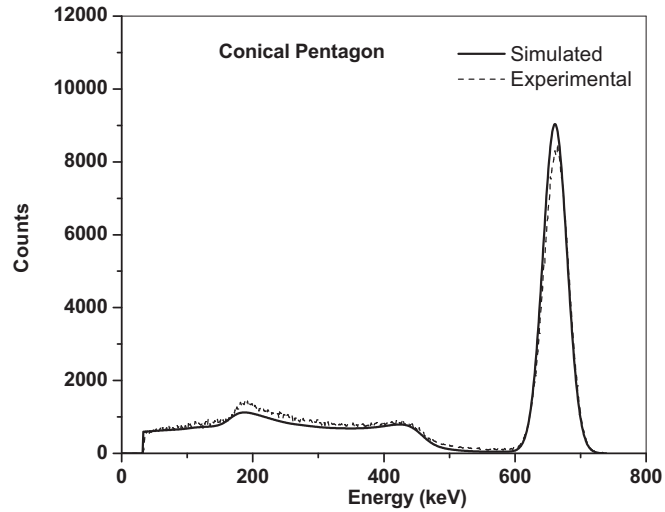

FIG. 3. ^{137}Cs γ-ray spectra measured with an individual pentagon crystal.

by adjusting beam energies in the laboratory system to 85.7, 91.9, 100, 104.1, 108.2, 112.2, 117.4, and 121.4 MeV. The Coulomb barrier V_B equivalent in laboratory frame for both systems is about 86 MeV. The ^{208}Pb and ^{206}Pb targets of thickness 250 $\mu g/cm^2$ (97.9% enriched) and 350 $\mu g/cm^2$ (99.9% enriched), respectively, were sandwiched between carbon layers of thickness 40 $\mu g/cm^2$ (backing which faced the beam) and 10 $\mu g/cm^2$ (capping), respectively [17]. The recoil energy of the ERs at the focal plane was ≈1.5 MeV with optimized helium gas pressure (0.15 Torr) in HYRA and isobutane gas pressure (2.0 Torr) at the focal plane. To measure the Rutherford (elastically) scattered beam for normalizing the reaction cross sections, two silicon surface barrier detectors (SSBDs) were placed inside the target chamber at a distance of 45 mm and at angles of ±25° with respect to the beam direction. These detectors were also used to monitor and observe the beam tuning on the target. The optimization of HYRA electromagnetic configuration (field settings are energy 'E', mass 'm', and atomic number 'Z' dependent) using a Monte Carlo simulation program and actual field scanning to optimize for maximum transmission (efficiency) are explained in detail in recent works by our group and are presented in [18–22].

The TIFR 4π spin spectrometer consists of 32 elements of NaI(Tl) scintillation detectors [23] arranged in soccer-ball geometry surrounding the HYRA target chamber. The detectors are conical shaped with pentagonal and hexagonal cross sections to make a perfectly close-packed assembly in spherical, soccer-ball geometry. The array is used to detect the low energy nonstatistical γ rays from the rotational (decay cascade) states of the ERs to determine the angular momentum. For our in-beam measurements, 29 of the total 32 detectors of the array were used for allowing the beam inlet and outlet pipes and the target ladder. The total solid angle covered is around 86%. The performance of the individual detectors and the array as a whole were tested extensively using low energy γ ray sources. Figures 3–5 present typical γ-ray spectra measured with the individual pentagon and hexagon crystals and the full array as a whole, respectively. The measured spectra have been reproduced with the simulated spectra generated by Monte Carlo simulations using GEANT4 package [24]. The energy resolutions of the individual crystals at 662 keV (^{137}Cs line) varied from 7 to 8 %. We have also measured and simulated the total detection and photo peak efficiencies of the detectors and the array as a whole. The measured and simulated values are provided in Table I. The ERs were detected at focal plane of the HYRA using multiwire proportional counter (MWPC) of size ≈15 × ≈ 5 cm^2. Time-of-flight (TOF) technique was used to obtain the cleanly separated ER events. For this we used two time-to-amplitude converters (TACs). First one was between MWPC-anode as start signal and RF-TAC as stop signal. Another one was between MWPC-anode as start signal and logic 'OR' signal of all the NaI(Tl) detectors of 4π spin spectrometer as stop signal. The logic 'OR' signals of the right monitor (MR), and the left monitor (ML) and anode MWPC signal were used as the master strobe for the data acquisition. Data were collected and analyzed using the CANDLE

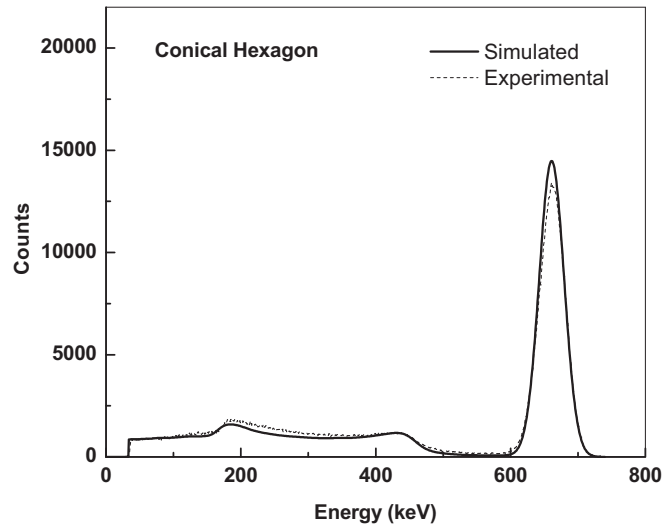

FIG. 4. ^{137}Cs γ-ray spectra measured with an individual hexagon crystal.

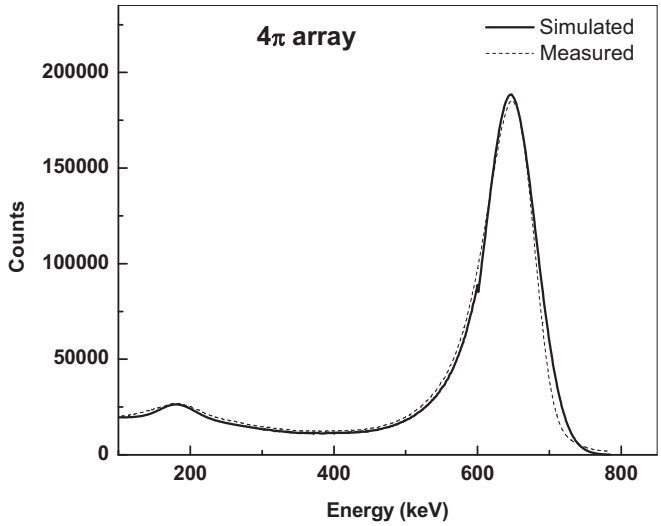

FIG. 5. ^{137}Cs γ-ray spectra measured with the full array as a whole.

(Collection and Analysis of Nuclear Data using Linux nEtwork) software package developed at the IUAC [25]. The details about the data analysis are given in the next section.

III. ANALYSIS AND RESULTS

The measurements were performed at the energies given in Table II for both reactions. Field scanning was done at each beam energy and, HYRA settings were optimized for maximum transmission of ERs by monitors yield ratio. The time taken by the ERs to traverse the distance from the target to the focal plane detector (MWPC) was ≈2.9 to ≈4 μs in the chosen energy range. The time of arrival technique gave a clean separation of ERs from the beam-like particles (or target-like recoils) and also from the noise generated by the focal plane strobe. Figure 2, shows a typical two-dimensional plot of the well separated ERs. The selected ERs were used for further data analysis.

TABLE I. Measured and simulated efficiencies for the detection systems using ^{137}Cs γ line.

Detection system	Total efficiency (%)		Photopeak efficiency (%)	
	Measured	Simulated	Measured	Simulated
conical pentagon (3 in. long)	2.06 ± 0.10	2.00 ± 0.03	1.03 ± 0.05	1.06 ± 0.03
conical hexagon (3 in. long)	3.03 ± 0.15	2.98 ± 0.03	1.63 ± 0.08	1.70 ± 0.04
4π array as a whole	77.7 ± 3.9	78.2 ± 1.1	55.3 ± 2.4	57.7 ± 1.3

TABLE II. HYRA transmission efficiencies for the reactions ^{16}O + ^{208}Pb and ^{18}O + ^{206}Pb at different energies scaled from the nearby energies of the calibration reaction.

Reaction system	E_{lab} (MeV)	$E_{c.m.}$ (MeV)	E^* (MeV)	η_{HYRA} (%)
^{16}O + ^{208}Pb	87.0	80.7	34.3	0.224 ± 0.045
	93.2	86.5	40.1	0.220 ± 0.044
	99.3	92.2	45.8	0.146 ± 0.029
	105.5	97.9	51.5	0.144 ± 0.028
	113.5	105.3	59.0	0.135 ± 0.027
	122.6	113.8	67.3	0.137 ± 0.027
^{18}O + ^{206}Pb	85.7	78.8	34.3	0.230 ± 0.046
	91.9	84.5	40.0	0.234 ± 0.047
	100.0	91.9	47.4	0.162 ± 0.032
	104.1	95.7	51.1	0.178 ± 0.035
	108.2	99.5	54.9	0.171 ± 0.034
	112.2	103.2	58.8	0.166 ± 0.033
	117.4	107.9	63.4	0.160 ± 0.032
	121.4	111.6	67.0	0.156 ± 0.031

A. HYRA transmission efficiency

The determination of the ER cross sections crucially depends upon the transmission efficiency of HYRA. A scaling method was adopted to estimate the transmission efficiency of HYRA for the ^{16}O + ^{208}Pb and ^{18}O + ^{206}Pb reactions. We have chosen the ^{16}O + ^{197}Au as a calibration reaction whose absolute ER excitation function is well studied and reported by several groups [10,26,27]. We have scaled the efficiencies for our reactions by the measured efficiencies of the calibration reaction. Measurement for the above mentioned calibration system was carried out at different laboratory energies with optimized parameters of HYRA. The experimentally measured efficiencies for ^{16}O + ^{197}Au at different laboratory energies are given in Table III. The transmission efficiency was measured for the calibration system using the expression given below:

$$\eta_{HYRA} = \frac{Y_{ER}}{Y_{\text{mon}}}\left(\frac{d\sigma}{d\Omega}\right)_R \Omega_{\text{mon}} \frac{1}{\sigma_{ER}}, \quad (1)$$

where η_{HYRA} is the transmission efficiency of HYRA recoil mass separator, Y_{ER} and Y_{mon} are proper yields acquired in the focal plane detector (MWPC) and monitor detectors $[\sqrt{(Y_{ML} \times Y_{MR})}]$, respectively. The elastically (Coulomb) scattered cross section is given as differential

TABLE III. The experimentally measured HYRA transmission efficiencies for the calibration reaction ^{16}O + ^{197}Au at different energies with the reported absolute ER cross sections in the literature.

Calibration system	E_{lab} (MeV)	σ_{ER} (mb)[10]	η_{HYRA}(%)
^{16}O + ^{197}Au	93.4	163.8	0.133 ± 0.026
	99.5	131.1	0.145 ± 0.029
	105.6	98.9	0.164 ± 0.033
	113.7	67.8	0.160 ± 0.032

Rutherford scattering cross section $(\frac{d\sigma}{d\Omega})_R$ in the laboratory frame. $\Omega_{\rm mon}$ is the solid angle subtended by the monitor detector from the target center and is in Sr. σ_{ER} is the absolute ER cross section in *mb* for the given system at a particular laboratory energy. The differential Rutherford scattering cross section at fixed laboratory angle as a function of the energy in laboratory frame is expressed as

$$\left(\frac{d\sigma}{d\Omega}\right)_R = 1.296\left(\frac{Z_pZ_t}{E_{\rm lab}}\right)^2\left[\frac{1}{\sin^4\left(\frac{\theta_L}{2}\right)} - 2\left(\frac{M_p}{M_t}\right)^2 + \cdots\right], \tag{2}$$

where Z_p, Z_t and M_p, M_t are the atomic numbers and masses of the projectile and target of the reaction system, respectively. As mentioned above $E_{\rm lab}$ and θ_L are the energy of the incident projectile at target center and scattering angle of the projectile-like particles measured with the monitor detectors in the laboratory frame of reference, respectively.

The HYRA transmission efficiencies for the systems ^{16}O + ^{208}Pb and ^{18}O + ^{206}Pb are scaled from the calibration system ^{16}O + ^{197}Au with their nearby energy points. The calibration system and the studied systems are almost in the same mass region. Therefore, with scaled parameters of experimental setup the efficiency scaling from calibration system to actual system is a more reliable and appropriate method compared to γ line counting with and without coincident ER [28,29]. The transmission efficiencies of HYRA for the systems ^{16}O + ^{208}Pb and ^{18}O + ^{206}Pb are given in Table II. For the transmission efficiency scaling, the ER angular distribution was simulated for calibration as well as reaction systems using PACE4 [30,31] Monte Carlo simulation code. The total ER angular distributions were considered for all the systems up to 9.5° of mass spectrometer angular acceptance. The simulated total ER angular distribution was compared with the other simulation code TERS [32,33] at higher energies. TERS is usually meant for the ER angular distribution, mass and charge distributions in recoil mass separators and have been used conventionally in previous works [18–22]. Once the transmission efficiencies of HYRA are estimated precisely for the measured systems, it is easy to extract the absolute ER cross sections for the same systems.

B. Total absolute ER cross sections

The total absolute ER cross section for the above measured systems is defined using the expression given below:

$$\sigma_{ER} = \frac{Y_{ER}}{Y_{\rm mon}}\left(\frac{d\sigma}{d\Omega}\right)_R \Omega_{\rm mon}\frac{1}{\eta_{HYRA}}. \tag{3}$$

The parameters for the above expression have already been discussed. Their values and the transmission efficiency η_{HYRA} are used here for the corresponding systems. The total fusion cross section is the sum of all the fusion-evaporation residue cross sections and the total fusion-fission cross section [34]. For the system ^{16}O + ^{208}Pb few measurements have reported the total fusion cross section [11,35] and the fission cross section [8,9]. Even though fusion-evaporation residue cross sections have been reported by few labs [7,9–11], there are discrepancies in the measured values. Most of them have reported ER cross sections for below and sub-barrier energies. To the best of our knowledge, so far, no fusion-evaporation residue measurements have been reported for the ^{18}O + ^{206}Pb reaction. The total absolute ER cross sections for the systems ^{16}O + ^{208}Pb and ^{18}O + ^{206}Pb are given in Table IV. The total absolute ER cross sections are plotted in Fig. 6 for both the systems as a function of excitation energy. The beam energies have been chosen to populate the CN ^{224}Th* at nearly same excitation energies for both reactions.

TABLE IV. The absolute total ER cross sections for the systems ^{16}O + ^{208}Pb and ^{18}O + ^{206}Pb.

Reaction system	$E_{\rm lab}$ (MeV)	$E_{\rm c.m.}$ (MeV)	E^* (MeV)	σ_{ER} (mb)
^{16}O + ^{208}Pb	87.0	80.7	34.3	4.7 ± 0.9
	93.2	86.5	40.1	4.9 ± 0.9
	99.3	92.2	45.8	14.5 ± 2.9
	105.5	97.9	51.5	9.0 ± 1.8
	113.5	105.3	59.0	8.7 ± 1.7
	122.6	113.8	67.3	12.5 ± 2.5
^{18}O + ^{206}Pb	85.7	78.8	34.3	4.2 ± 0.8
	91.9	84.5	40.0	5.8 ± 1.1
	100.0	91.9	47.4	10.8 ± 2.1
	104.1	95.7	51.1	10.2 ± 2.0
	108.2	99.5	54.9	12.8 ± 2.5
	112.2	103.2	58.8	16.8 ± 3.3
	117.4	107.9	63.4	18.5 ± 3.7
	121.4	111.6	67.0	19.8 ± 3.9

C. Efficiency of 4π spin spectrometer array

The TIFR 4π spin spectrometer has been used to determine the ER spin distributions by measuring the γ multiplicity for de-exciting CN ^{224}Th*. The multiplicity filter covers nearly 86% of the total 4π geometry [23,24,36,37]. In the present set of measurements, 29 of the total 32 detectors have been used.

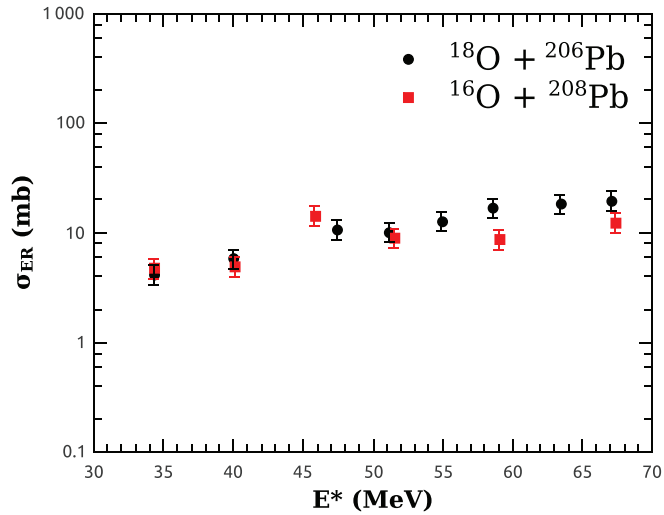

FIG. 6. The evaporation residue excitation functions for the systems ^{16}O + ^{208}Pb and ^{18}O + ^{206}Pb.

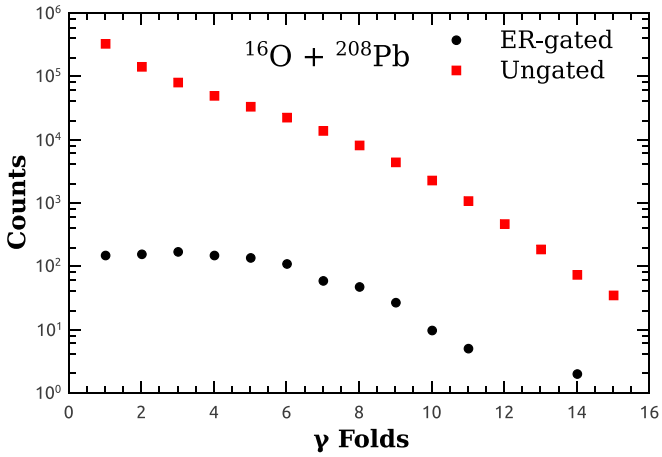

FIG. 7. ER-gated and ungated γ fold distributions for the ^{16}O + ^{208}Pb reaction at E_{lab} = 99.3 MeV.

Out of these, ten have pentagonal and 19 are of hexagonal cross sectional geometry. The detection efficiencies of the pentagonal and hexagonal detectors are 2.08% and 3.05%, respectively at 661.7 keV [37]. At closed position, the inner diameter of the soccer-ball geometry restricts the scattering chamber to 12 cm in diameter. For the determination of the CN angular momentum distribution the gamma multiplicity distribution is to be corrected by the detector efficiency. The efficiency of the complete array has been estimated at Cs-137 and Co-60 γ ray energies (661.7, 1173.2, and 1332.5 keV) by successively placing the radioactive sources at the center of the sphere. The efficiencies have also been simulated with the GEANT4 Monte Carlo simulation code [24].

D. ER-gated spin distributions

The raw γ-fold distribution spectra were obtained at each energy from the 29 detectors. The timing signals from all the detectors were matched in time using suitable delays. The thresholds were set at around 100 keV (below the expected energies of the gamma-rays and above the x-ray energies). The time-matched 'OR' signal of all the detectors and the multiplicity signal were generated from the multichannel constant fraction discriminators. The raw γ-fold distribution has contributions from both the nonstatistical stretched transitions of the rotating ERs as well as nonrotational, statistical γ rays, and γ rays from carbon and contamination in the target. To remove contaminating non-ER contributions, we generated the γ-fold distributions by gating with the ERs. The γ-fold distributions (ER-gated and ungated) are shown in Fig. 7.

In the present work, the ER-gated spin distributions for ^{16}O + ^{208}Pb and ^{18}O + ^{206}Pb were extracted from the experimental ER-gated γ-fold distributions. In this study, we have generated the response matrix for the 4π spin spectrometer with respect to its geometry using GEANT4 Monte Carlo simulation [38,39]. The detector response matrix fold distribution for various fixed γ multiplicities are shown in Fig. 8. This figure plots the results of our simulations for the observed fold (k) distributions for M (multiplicity) number of uncorrelated γ rays in an array of N detectors in compact 4π soccer-ball

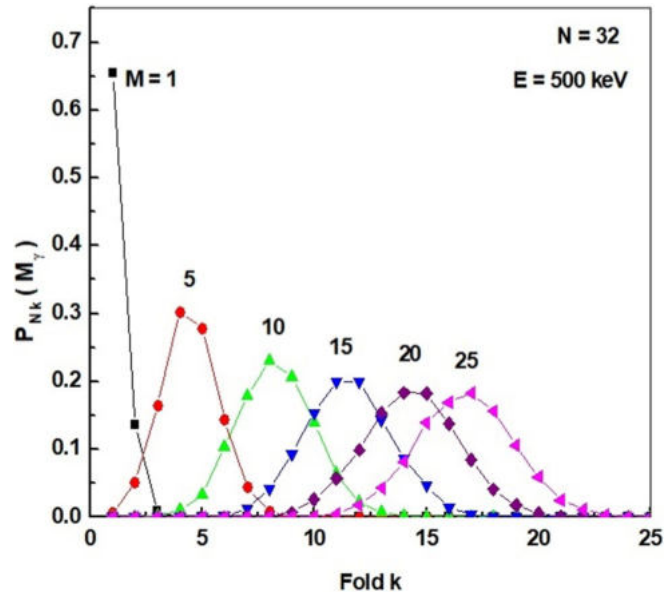

FIG. 8. GEANT4 simulated fold distribution for the spin spectrometer for different γ multiplicities.

configuration. In this simulation, we have considered $N = 32$ and average energy of 500 keV for the γ rays. We have also performed the simulation for 29 detectors which is the actual number used in our measurements. The response function $R(k, M_\gamma)$ has been convoluted with a chosen spin distribution to reproduce the experimentally obtained fold distribution. Here, we have assumed that the chosen γ-multiplicity distribution $P(M_\gamma)$ is similar to the Fermi-function distribution and it is expressed as

$$P(M_\gamma) = \frac{2M_\gamma + 1}{\exp\left(\frac{M_\gamma - M_0}{\Delta M}\right) + 1}, \tag{4}$$

where M_0 and ΔM are the free parameters in multiplicity distribution to fit the experimental fold distribution. In such

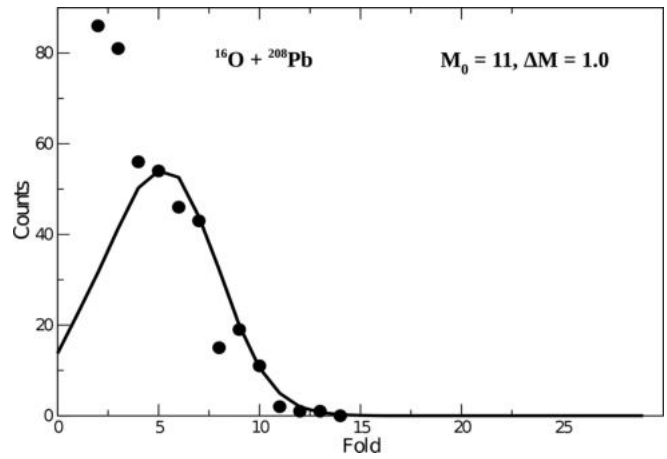

FIG. 9. The experimental and simulated fold distributions for ^{16}O + ^{208}Pb at E^* = 40.0 MeV.

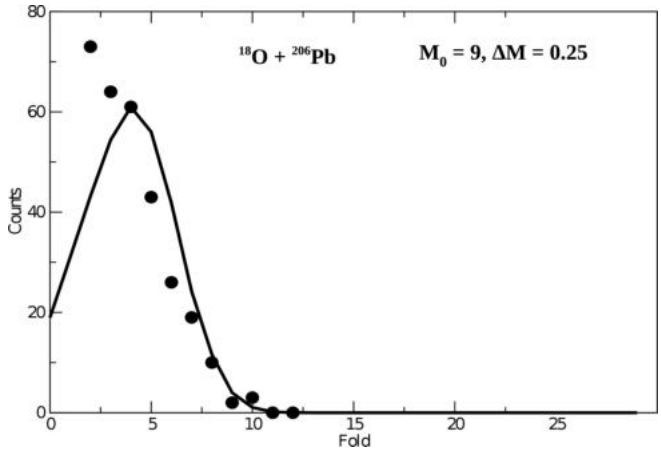

FIG. 10. The experimental and simulated fold distributions for ^{18}O + ^{206}Pb at E* = 40.1 MeV.

a case, the fold distribution $P(k)$ can be written as

$$P(k) = \sum_{M_\gamma=0}^{\infty} R(k, M_\gamma) P(M_\gamma), \tag{5}$$

where, by convolution of $R(k, M_\gamma)$ and $P(M_\gamma)$, the fold distribution is constructed. The simulated fold distribution is fitted to the experimental fold distribution by varying the parameters M_0 and ΔM. Two representative plots for both the reactions are shown in Figs. 9 and 10. Table V presents the fitted values of M_0 and ΔM for both the reactions at various beam energies. It is worth noting that there is an increase in the most probable value of the spin distribution (M_0) with increase in beam energy.

IV. SUMMARY AND CONCLUSION

The measurements of ER cross sections and spin distributions for ^{16}O + ^{208}Pb and ^{18}O + ^{206}Pb were carried out using the HYRA recoil mass separator coupled with the TIFR 4π γ ray spin spectrometer facility at IUAC. The CN ^{224}Th* was populated at similar excitation energies through two different

TABLE V. The fitted Fermi-function free parameters for ^{16}O + ^{208}Pb and ^{18}O + ^{206}Pb.

Reaction system	$E_{c.m.}$ (MeV)	E^* (MeV)	Fermi-function free parameters M_0	ΔM
^{16}O + ^{208}Pb	80.7	34.3	11	1.0
	86.5	40.1	11	1.0
	92.2	45.8	11	0.75
	97.9	51.5	12	0.25
	105.3	59.0	17	1.0
	113.8	67.3	16	1.0
^{18}O + ^{206}Pb	78.8	34.3	8	0.5
	84.5	40.0	9	0.25
	111.6	67.0	10	1.0

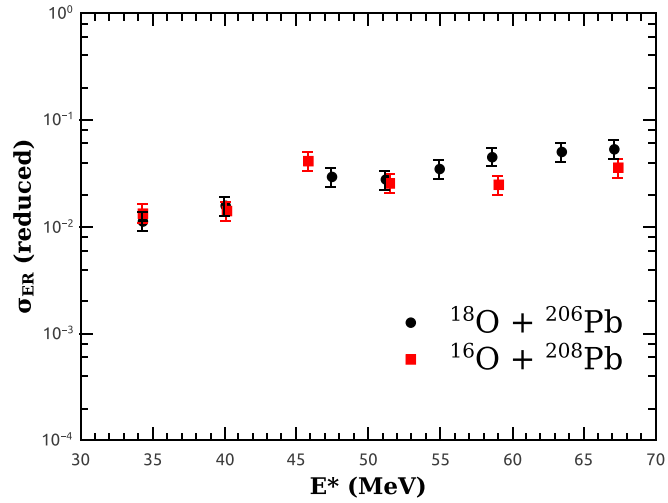

FIG. 11. Reduced ER cross sections ($\sigma_{ER}/\pi R_B^2$) at given excitation energies for the two reactions.

entrance channels with nominal difference in the projectile and target combination. From the ER cross sections extracted from both the reactions, it can be observed that the survival probability of ERs against fission is almost same for both systems at low excitation energies while the ER cross sections for ^{18}O + ^{206}Pb system are slightly higher at higher excitation energies (Fig. 11). The efficiency corrected absolute ER cross sections for the ^{16}O + ^{208}Pb system is compared with the previous results [7,9–11] measured with different techniques in Fig. 12. Our data match quite well with the reported cross sections of Brinkmann *et al.* [10] above 95 MeV laboratory energy. However, the two sets vary below 95 MeV. The data of Vulgaris *et al.* [9] and Morton *et al.* [11] vary significantly from both our data and that of Brinkmann [10]. Unlike the previous measurements we have also extracted the spin distributions. The spin distributions shift towards the higher values with increased beam energy. We also report, for the

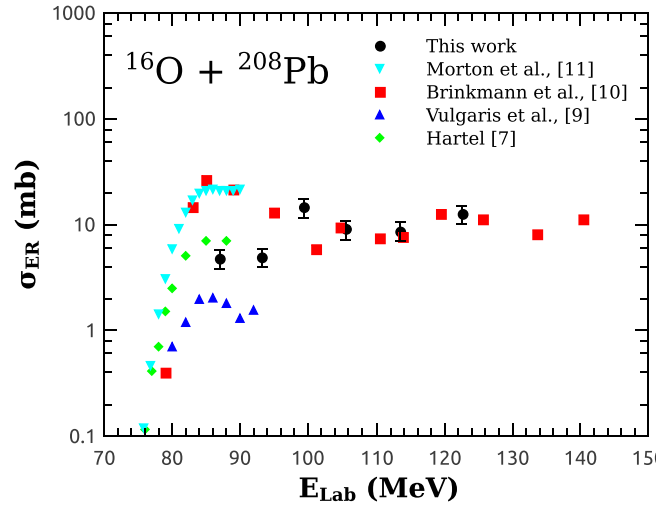

FIG. 12. The experimental absolute ER cross sections measured with different techniques.

first time, ER cross sections and ER-gated spin distributions for the $^{18}O + ^{206}Pb$ reaction leading to the same ^{224}Th CN. We observe that the ER cross sections for the two systems are nearly equal at low excitation energies but the $^{18}O + ^{206}Pb$ exhibits higher ER cross sections at higher excitation energies. However, $^{18}O + ^{206}Pb$ reaction shows lower ER gated mean γ ray multiplicities at all excitation energies which implies smaller l_{CN} (mean angular momentum) values, contrary to expectation. The primary objective of this work has been the experimental determination of the ER-gated angular momentum distributions and ER cross sections for two different reactions leading to the same CN at similar excitation energies. We have presented the primary experimental observations and the immediate inferences. A fuller analysis of the results using both statistical model and dynamical calculations are currently being carried out and will be presented in a future communication.

ACKNOWLEDGMENTS

The Pelletron and the LINAC groups are acknowledged for providing good quality pulsed beams during the experiment. One of the authors (M.M.H.), would like to thank IUAC, New Delhi for financial support (UFR-51312 sanctioned to N.M.B.). Also thanks to IUAC target laboratory and RBS laboratory for fabrication of isotopically enriched thin targets and their characterization. Authors would like to thank Dr. S. Pal for valuable discussions regarding this work.

[1] P. Fröbrich and I. I. Gontchar, Nucl. Phys. A **563**, 326 (1993).
[2] I. Diószegi, N. P. Shaw, I. Mazumdar, A. Hatzikoutelis, and P. Paul, Phys. Rev. C **61**, 024613 (2000).
[3] N. P. Shaw, I. Diószegi, I. Mazumdar, A. Buda, C. R. Morton, J. Velkovska, J. R. Beene, D. W. Stracener, R. L. Varner, M. Thoennessen, and P. Paul, Phys. Rev. C **61**, 044612 (2000).
[4] H. Rossner, D. J. Hinde, J. R. Leigh, J. P. Lestone, J. O. Newton, J. X. Wei, and S. Elfström, Phys. Rev. C **45**, 719 (1992).
[5] Louis C. Vaz, D. Logan, E. Duek, John M. Alexander, M. F. Rivet, M. S. Zisman, Morton Kaplan, and J. W. Ball, Z. Phys. A At. Nucl. **315**, 169 (1984).
[6] B. J. Fineman, K.-T. Brinkmann, A. L. Caraley, N. Gan, R. L. McGrath, and J. Velkovska, Phys. Rev. C **50**, 1991 (1994).
[7] K. Hartel, Ph. D. thesis, Technical University of Munich, 1985 (unpublished).
[8] T. Murakami, C.-C. Sahm, R. Vandenbosch, D. D. Leach, A. Ray, and M. J. Murphy, Phys. Rev. C **34**, 1353 (1986).
[9] E. Vulgaris, L. Grodzins, S. G. Steadman, and R. Ledoux, Phys. Rev. C **33**, 2017 (1986).
[10] K.-T. Brinkmann, A. L. Caraley, B. J. Fineman, N. Gan, J. Velkovska, and R. L. McGrath, Phys. Rev. C **50**, 309 (1994).
[11] C. R. Morton, D. J. Hinde, J. R. Leigh, J. P. Lestone, M. Dasgupta, J. C. Mein, J. O. Newton, and H. Timmers, Phys. Rev. C **52**, 243 (1995).
[12] I. Mazumdar, Pramana - J. Phys. **85**, 357 (2015).
[13] A. K. Nasirov, B. M. Kayumov, G. Mandaglio, G. Giardina, K. Kim, and Y. Kim, Eur. Phys. J. A **55**, 29 (2019).
[14] N. Madhavan, S. Nath, T. Varughese, J. Gehlot, A. Jhingan, P. Sugathan, A. K. Sinha, R. Singh, K. M. Varier, M. C. Radhakrishna, E. Prasad, S. Kalkal, G. Mohanto, J. J. Das, Rakesh Kumar, R. P. Singh, S. Muralithar, R. K. Bhowmik, A. Roy, Rajesh Kumar, S. K. Suman, A. Mandal, T. S. Datta, J. Chacko, A. Choudhury, U. G. Naik, A. J. Malyadri, M. Archunan, J. Zacharias, S. Rao, Mukesh Kumar, P. Barua, E. T. Subramanian, K. Rani, B. P. Ajith kumar, and K. S. Golda, Pramana - J. Phys. **75**, 317 (2010).
[15] N. Madhavan, I. Mazumdar, T. Varughese, J. Gehlot, S. Nath, D. A. Gothe, P. B. Chavan, G. Mohanto, M. B. Naik, I. Mukul, and A. K. Sinha, EPJ Web Conf. **17**, 14003 (2011).
[16] G. Anil Kumar, I. Mazumdar, and D. A. Gothe, in *IEEE Nuclear Science Symposium Conference*, Record No. N17-1, p. 1640 (IEEE, 2008).
[17] M. M. Hosamani, S. R. Abhilash, S. Ojha, G. R. Umapathy, N. M. Badiger, and D. Kabiraj, J. Instrum. **14**, 01007 (2019).
[18] E. Prasad, K. M. Varier, N. Madhavan, S. Nath, J. Gehlot, Sunil Kalkal, Jhilam Sadhukhan, G. Mohanto, P. Sugathan, A. Jhingan, B. R. S. Babu, T. Varughese, K. S. Golda, B. P. Ajith Kumar, B. Satheesh, Santanu Pal, R. Singh, A. K. Sinha, and S. Kailas, Phys. Rev. C **84**, 064606 (2011).
[19] Varinderjit Singh, B. R. Behera, Maninder Kaur, A. Kumar, K. P. Singh, N. Madhavan, S. Nath, J. Gehlot, G. Mohanto, A. Jhingan, Ish Mukul, T. Varughese, Jhilam Sadhukhan, Santanu Pal, S. Goyal, A. Saxena, S. Santra, and S. Kailas, Phys. Rev. C **89**, 024609 (2014).
[20] R. Sandal, B. R. Behera, Varinderjit Singh, Maninder Kaur, A. Kumar, Gurpreet Kaur, P. Sharma, N. Madhavan, S. Nath, J. Gehlot, A. Jhingan, K. S. Golda, Hardev Singh, S. Mandal, S. Verma, E. Prasad, K. M. Varier, A. M. Vinodkumar, A. Saxena, J. Sadhukhan, and S. Pal, Phys. Rev. C **91**, 044621 (2015).
[21] A. Shamlath, E. Prasad, N. Madhavan, P. V. Laveen, J. Gehlot, A. K. Nasirov, G. Giardina, G. Mandaglio, S. Nath, Tathagata Banerjee, A. M. Vinodkumar, M. Shareef, A. Jhingan, T. Varughese, DVGRKS Kumar, P. S. Devi, Khushboo, P. Jisha, Neeraj Kumar, M. M. Hosamani, and S. Kailas, Phys. Rev. C **95**, 034610 (2017).
[22] P. Sharma, B. R. Behera, Ruchi Mahajan, Meenu Thakur, Gurpreet Kaur, Kushal Kapoor, Kavita Rani, N. Madhavan, S. Nath, J. Gehlot, R. Dubey, I. Mazumdar, S. M. Patel, M. Dhibar, M. M. Hosamani, Khushboo, Neeraj Kumar, A. Shamlath, G. Mohanto, and S. Pal, Phys. Rev. C **96**, 034613 (2017).
[23] I. Mazumdar, DAE Symp. on Nucl. Phys. **53**, 713 (2008).
[24] G. Anil Kumar, I. Mazumdar, and D. A. Gothe, Nucl. Instrum. Methods Phys. Res. A **611**, 76 (2009).
[25] E. T. Subramanium, http://www.iuac.res.in/NIAS.
[26] S. Baba, K. Hata, S. Ichikawa, T. Sekine, Y. Nagame, A. Yokoyama, M. Shoji, T. Saito, N. Takahashi, H. Baba, and I. Fujiwara, Z. Phys. A At. Nucl. **331**, 53 (1988).
[27] L. Corradi, B. R. Behera, E. Fioretto, A. Gadea, A. Latina, A. M. Stefanini, S. Szilner, M. Trotta, Y. Wu, S. Beghini, G. Montagnoli, F. Scarlassara, R. N. Sagaidak, S. N. Atutov, B. Mai, G. Stancari, L. Tomassetti, E. Mariotti, A. Khanbekyan, and S. Veronesi, Phys. Rev. C **71**, 014609 (2005).
[28] P. D. Shidling, N. M. Badiger, S. Nath, R. Kumar, A. Jhingan, R. P. Singh, P. Sugathan, S. Muralithar, N. Madhavan, A. K. Sinha, Santanu Pal, S. Kailas, S. Verma, K. Kalita, S. Mandal, R. Singh, B. R. Behera, K. M. Varier, and M. C. Radhakrishna, Phys. Rev. C **74**, 064603 (2006).

[29] P. D. Shidling, N. Madhavan, V. S. Ramamurthy, S. Nath, N. M. Badiger, Santanu Pal, A. K. Sinha, A. Jhingan, S. Muralithar, P. Sugathan, S. Kailas, B. R. Behera, R. Singh, K. M. Varier, and M. C. Radhakrishna, Phys. Lett. B **670**, 99 (2008).
[30] O. B. Tarasov and D. Bazina, Nucl. Insrum. Methods Phys. Res. B **266**, 4657 (2008).
[31] A. Gavron, Phys. Rev. C **21**, 230 (1980).
[32] S. Nath, Comput. Phys. Commun. **179**, 492 (2008).
[33] S. Nath, Comput. Phys. Commun. **180**, 2392 (2009).
[34] T. Banerjee, S. Nath, and S. Pal, Phys. Rev. C **91**, 034619 (2015).
[35] B. B. Back, R. R. Betts, J. E. Gindler, B. D. Wilkins, S. Saini, M. B. Tsang, C. K. Gelbke, W. G. Lynch, M. A. McMahan, and P. A. Baisden, Phys. Rev. C **32**, 195 (1985).
[36] G. Mohanto, N. Madhavan, S. Nath, J. Sadhukhan, J. Gehlot, I. Mazumdar, M. B. Naik, E. Prasad, I. Mukul, T. Varughese, A. Jhingan, R. K. Bhowmik, A. K. Sinha, D. A. Gothe, P. B. Chavan, S. Pal, V. S. Ramamurthy, and A. Roya, Nucl. Phys. A **890–891**, 62 (2012).
[37] G. Mohanto, N. Madhavan, S. Nath, J. Gehlot, Ish Mukul, A. Jhingan, T. Varughese, A. Roy, R. K. Bhowmik, I. Mazumdar, D. A. Gothe, P. B. Chavan, J. Sadhukhan, S. Pal, Maninder Kaur, Varinderjit Singh, A. K. Sinha, and V. S. Ramamurthy, Phys. Rev. C **88**, 034606 (2013).
[38] J. Allison, K. Amako, J. Apostolakis, H. Araujo, P. Arce Dubois, M. Asai, G. Barrand, R. Capra, S. Chauvie, R. Chytracek, G. A. P. Cirrone, G. Cooperman, G. Cosmo, G. Cuttone, G. G. Daquino, M. Donszelmann, M. Dressel, G. Folger, F. Foppiano, J. Generowicz, V. Grichine, S. Guatelli, P. Gumplinger, A. Heikkinen, I. Hrivnacova, A. Howard, S. Incerti, V. Ivanchenko, T. Johnson, and F. Jones, IEEE Trans. Nucl. Sci. **53**, 270 (2006).
[39] J. Allison *et al.*, Nucl. Instrum. Methods Phys. Res. A **835**, 186 (2016).